Comparative Presentation of Criteria for Adaptive Finite-Element Mesh Generation in Multiconductor Eddy-Current Problems

Dimitris P. Labridis, *Member, IEEE*

***Abstract*—Four local error estimators used for *a posteriori* h-type adaptive finite-element mesh generation are presented and compared in the solution of several steady-state multiconductor eddy-current problems, encountered in electrical power transmission and distribution systems. The proposed technique combines four different criteria with the concept of Delaunay triangulation to provide finite-element triangular meshes, adaptive to the characteristics of each problem. By refining the elements with the largest errors and recomputing the solution iteratively, finite-element meshes having a uniform error density are obtained. The problems examined lead to quantitative results concerning the performance of each estimator in the accuracy of the solution, in terms of both convergence rate and quality of electromagnetic field lines.**

***Index Terms*—Adaptive systems, eddy currents, finite-element methods, multiconductor transmission lines.**

I. Introduction

DEVELOPED first in the domain of structural analysis [1], *a posteriori* error estimation leading to an h-type adaptive meshing turned out to be [2] an essential part of all finite-element procedures used to solve electrostatic and magnetostatic problems. Error estimators have been originally introduced in the literature in conjunction with adaptive mesh methodologies in [3]. The proposed methods fall into two basic categories:

- error estimators based on dual or complementary variational principles [3]–[5] and
- error estimators based on the requirement of equidistribution of various locally estimated norms and/or functions [5]–[11].

The former approach requires, however, a second solution at every step of the iterative procedure, by implementing an additional formulation for the complementary problem. In general, procedures based on dual or complementary solutions are slow and difficult to implement [8], especially for three-dimensional (3–D) problems. Therefore, local error estimators seem to be in general the best option.

The mesh optimization and, therefore, the quality assessment of the solution depends on the choice of the suitable error estimator. Due to the large number of proposed heuristic estimators, a comparative evaluation of performance of adaptive meshing algorithms using different estimators is useful [12]–[14], in order to choose the suitable estimator for a particular electromagnetic field problem. The correct choice is further complicated by the fact that these estimators tend to be problem-oriented. Examples of exclusive applications to distinct electrical engineering areas are problems with saturable ferromagnetic regions [15], analysis of microwave and optical devices [16], inverse and forward biomagnetic problems [17], dipole and quadruple magnets [18].

Application of error estimators exclusively to steady state time harmonic quasi-static eddy-current problems have also been recently reported [19]–[22]. The most significant difference with respect to the corresponding techniques developed for magnetotstatics is that phasor quantities are involved in modelling steady state, as a response to a time harmonic excitation current. As a result, some error indicators do not maintain a constant value during the period of the current. The time variation of these estimators must therefore be taken into account, in order to increase their reliability.

In this paper, an investigation on four different *a posteriori* error estimators has been performed, limited to triangular first-order elements. Results have been analyzed and compared, in the solution of several two–dimensional (2-D) multiconductor eddy-current problems commonly encountered in power systems. Therefore, the 2-D formulation of [23], [24] has been considered, in order to impose the known rms currents flowing through each conductor. Another approach, suggested in [32], [33], is directly extendable to three-dimensional (3-D) multiconductor eddy-current problems and it could be used in the case of a 3-D generalization of the proposed estimators.

Numerical examples examined include overhead transmission lines, underground power cables, and substation busbars under various loading conditions. In every example, characteristic operational parameters are computed and compared to corresponding values obtained from analytical solutions. Useful conclusions are obtained from this comparison and finally a single local error estimator is proposed as being more suitable for all the above mentioned problems.

II. Interelement Conditions

A. Global Boundary Relations

The well-known [23], [24] diffusion equation governing 2-D multiconductor eddy-current problems in the complex domain is

$$\frac{1}{\mu_0\mu_r}\left[\frac{\partial^2 A_z(x,y)}{\partial x^2}+\frac{\partial^2 A_z(x,y)}{\partial y^2}\right] - j\omega\sigma A_z(x,y)+J_{sz}=0$$

$$-j\omega\sigma A_z(x,y)+J_{sz}=J_z(x,y) \qquad (1a)$$

Manuscript received January 15, 1999; revised September 1, 1999.

The author is with the Power Systems Laboratory, Department of Electrical and Computer Engineering, Aristotle University of Thessaloniki, GR-54006, Thessaloniki, Greece (e-mail: labridis@eng.auth.gr).

Publisher Item Identifier S 0018-9464(00)00472-6.

along with the necessary boundary conditions in the limit C of the solution region S

$$A_z(x, y)|_C = A_0(x, y) \tag{1b}$$

and

$$\iint_S J_z(x, y)ds = I_{\rm rms} \tag{1c}$$

where

μ_0 the permeability of vacuum;
μ_r the relative permeability;
J_{sz} the z-direction component of the uniformly distributed source current density;
$I_{\rm rms}$ the rms current flowing through each conductor.

The unknowns in the systems of (1a) are A_z and J_{sz}, the values of A_z at the limit C of region S are specified by the Dirichlet condition (1b), and the total current density J_z is specified by the integral form (1c).

Multiconductor eddy-current problems encountered in power systems always consist of many interconnected materials, and therefore, it is required to satisfy the interface relations. These are the continuity of the normal component of the flux density vector $\vec{B}$ and the continuity of the tangential components of the magnetic field vector $\vec{H}$ across the boundary between two different materials. In the 2-D formulation of the diffusion equation (1a)–(1c) it is supposed that the only component of magnetic vector potential (MVP) is in the z direction, i.e.,

$$\vec{A} = \vec{z}_0 A_z(x, y) \tag{2a}$$

where A_z is a complex phasor, since the excitation current is supposed to be harmonic. Using the definition of MVP, it can be easily shown that

$$\begin{aligned} \boldsymbol{B} &= \boldsymbol{x}_0 \frac{\partial A_z(x, y)}{\partial y} - \boldsymbol{y}_0 \frac{\partial A_z(x, y)}{\partial x} \\ &= \boldsymbol{x}_0 B_x(x, y) + \boldsymbol{y}_0 B_y(x, y) \end{aligned} \tag{2b}$$

$$|\nabla A_z| = \left|\nabla \times \vec{A}\right| = \left|\vec{B}\right| \tag{2c}$$

and

$$\nabla A_z \cdot \nabla \times \vec{A} = 0 \tag{2d}$$

where the flux density components B_x and B_y are also complex phasors. However, the absolute value of the resultant flux density at a point, given from (2b) and (2c), is obviously a complex number but *not a phasor*. This is the major difficulty of the estimators encountered in eddy-current problems, as it will be shown later.

In any case, the continuity of the normal component of the flux density in terms of MVP may be written as

$$(\nabla A_z)_{t1} = (\nabla A_z)_{t2} \tag{3a}$$

and that of the tangential component of the magnetic field as

$$\frac{1}{\mu_1}(\nabla A_z)_{n1} = \frac{1}{\mu_2}(\nabla A_z)_{n2} \tag{3b}$$

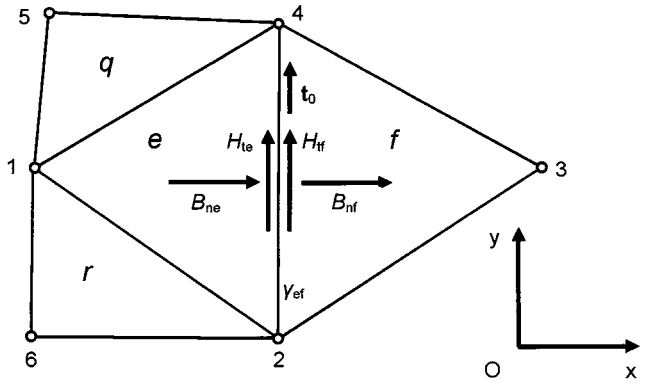

Fig. 1. A typical triangular element e and its neighbors f, q, and r.

across the boundary between materials one and two, having magnetic permeabilities μ_1 and μ_2, respectively.

B. Local Boundary Conditions in 2-D FEM Formulation

The application of boundary conditions in elementary level will be defined with the help of Fig. 1. Element e and one of its neighbors f belong in the general case to two different materials, with properties characterised by the subscripts e and f, respectively. Therefore, across their common side γ_{ef} the interface relations (3a) and (3b) must be verified.

Supposing for simplicity that first order finite elements are used and knowing that their shape functions are always continuous, the continuity relation of the normal component of the flux density across a is always preserved from the definition of the MVP as the curl of flux density vector $\vec{B}$, i.e.,

$$(\nabla A_z)_{te} = (\nabla A_z)_{tf} = \frac{A_2 - A_4}{\ell} \Rightarrow B_{ne} = B_{nf} = \frac{A_2 - A_4}{\ell} \tag{4a}$$

where ℓ is the length of γ_{ef}. On the contrary, the continuity relation of the tangential component of the magnetic field is a natural condition and it is obtained only in a mean sense [25]. This means that an error is always introduced in the application of (3b) across γ_{ef}, and this error is only minimized (although never vanishes) by a mesh having more and smaller elements in that area. Therefore, the quantity Q_{ef} given by

$$\begin{aligned} Q_{ef} &= \frac{1}{\mu_e}(\nabla A)_{ne} - \frac{1}{\mu_f}(\nabla A)_{nf} = \frac{1}{\mu_e}B_{te} - \frac{1}{\mu_f}B_{tf} \\ &= H_{te} - H_{tf} \end{aligned} \tag{4b}$$

is always nonzero and therefore it represents one of the most frequently used local error estimators.

A last but important remark concerning (4b) is that Q_{ef} is always a complex number, but not a phasor. It is well known that the locus of the absolute value of the resultant flux density, defined in a 2-D problem in (2b) and (2c), is an ellipse in the x–y plane. Moreover, since the field and physical properties of the two neighbors e and f are dissimilar, the corresponding ellipses differ significantly not only in their major and minor axes, but also in their orientation. Therefore, in order to estimate correctly the contribution of the local error introduced in (4b), the actual time variation of every component of Q_{ef} must be taken into account. This will lead to instantaneous and real values of

the error estimators, allowing greater flexibility in all necessary comparisons.

III. Error Estimators

Many error estimators have been proposed in the literature [11], [19], [20]–[22], for the solution of eddy-current problems. In this paper, four estimators are proposed and applied to the solution of various power transmission and distribution multiconductor problems. The first two estimators are based on the interelement conditions previously explained, while the other two are based on the equidistribution of the stored magnetic energy.

A. Criterion #1: Weighted Discontinuity of the Instantaneous Tangential Component H_t

Considering the typical element e, shown in Fig. 1 and assuming that $\boldsymbol{t}_0$ is the unit vector in the direction of the common side γ_{ef} between e and its neighbor f, an error estimator h_f may be defined, according to (4b), as

$$h_f = \iint_{S_e} \left(\left[\frac{1}{\mu_e} \boldsymbol{B}_e - \frac{1}{\mu_f} \boldsymbol{B}_f \right] \cdot \boldsymbol{t}_0 \right)^2 ds. \tag{5}$$

Corresponding error estimators h_q and h_r may be defined for the other two neighbors q and r of element e. The discontinuity of the two components is further weighted with the area S_e of element e, so that large elements obtain priority for refinement. This usually leads [9] to an increase of convergence of the adaptive procedure.

However, when power system quasi-static eddy-current problems are solved using the 2-D formulation of (1a)–(1c), complex quantities due to the harmonic current excitation are introduced. As a consequence, h_f of (5) will also be complex and not a phasor, as explained earlier. To overcome this, the actual time variation of the flux density will be considered here.

Assuming that only first order elements are employed in the 2-D finite-element method (FEM) analysis, constant complex flux densities are obtained by (2b) within each element. According to the notation of Fig. 1, the estimator defined in (5) becomes a complex number equal to

$$h_f = \left(\frac{1}{\mu_e} B_{te} - \frac{1}{\mu_f} B_{tf} \right)^2 S_e. \tag{6}$$

The x and y direction components of the constant elementary flux density may be written in terms of the rms values B_{xe} and B_{ye} and phase angles ϕ_{xe} and ϕ_{ye}, respectively. The corresponding harmonic time variation of every component of the elementary flux density will be

$$b_{xe}(t) = \sqrt{2} B_{xe} \cos(\omega t + \phi_{xe}) \tag{7a}$$

$$b_{ye}(t) = \sqrt{2} B_{ye} \cos(\omega t + \phi_{ye}) \tag{7b}$$

and the time variation of the magnitude of the elementary resultant flux density

$$|b_e(t)| = \sqrt{2} \Big[[B_{xe} \cos(\omega t + \phi_{xe})]^2 + [B_{ye} \cos(\omega t + \phi_{ye})]^2 \Big]^{1/2}. \tag{7c}$$

A time sampling is used, by dividing the period T into n_T equal intervals. Every time instant j corresponds to a time angle equal to $(j-1)d/n_T$ rads. Using this time angle, instantaneous values b_{ej} of the magnitude of the elementary flux density are computed at every time instant j using (7c). Tangential instantaneous components b_{tej}, b_{tfj} are then calculated in the common side γ_{ef} and a real and positive instantaneous estimator is defined from (6) as

$$h_{fj} = \left(\frac{1}{\mu_e} b_{tej} - \frac{1}{\mu_f} b_{tfj} \right)^2 S_e. \tag{8}$$

Real and positive estimators h_{qj} and h_{rj} similar to (8) may be easily expressed for the other two neighbors q and r of element e. At every j, a maximum elementary real error estimator is computed as

$$h_j = \max(h_{fj}, h_{qj}, h_{rj}). \tag{9}$$

By applying next a requirement of equidistribution of the error, which in many other cases [6] has been shown to lead to an optimal mesh, the mean value h_{mj} of all h_j defined in (9) is calculated at every time instant j, for all triangles of the current mesh. All triangles with $h_j \geq w h_{mj}$ are marked with a unitary integer flag, where w is a user defined integer parameter such that $w \geq 1$. The above procedure continues for all time intervals $j = 1, 2, \ldots, n_T$. In the end, every element e will be assigned a integer number equal to the sum of the corresponding n_T instantaneous integer flags, being therefore in the range [0–n_T].

The previous procedure is easily incorporated in the adaptation mechanism and has many advantages. First, it implies real only arithmetic. The second is that it gives the user the opportunity to experiment with the optimum number of time intervals, in order to accommodate time and memory resources of the computer. Finally, it ends up with a flexible error estimation, in the sense that the user is able to choose which of the triangles will be refined in the next mesh. Some of these choices may be, for example, to refine all the triangles set with error flag ≥ 1, or to refine only the triangles set with an error flag equal to n_T.

B. Criterion #2: Absolute Discontinuity of the Instantaneous Tangential Component H_t

This criterion is a variation of the previous one and it is also based on the discontinuity of the tangential component of the magnetic field, as defined in (4b). It emphasizes on the absolute difference of the two tangential components, completely ignoring the size of the corresponding element e. Following the notation of Fig. 1, an error estimation between e and f is now defined as

$$h_f = \left| \left[\frac{1}{\mu_e} \boldsymbol{B}_e - \frac{1}{\mu_f} \boldsymbol{B}_f \right] \cdot \boldsymbol{t}_0 \right|. \tag{10}$$

Assuming again first order elements and constant complex flux densities in every element, the estimator defined in (10) becomes in quasi-static eddy-current problems another complex quantity equal to

$$h_f = \left| \frac{1}{\mu_e} B_{te} - \frac{1}{\mu_f} B_{tf} \right|. \tag{11}$$

In order to overcome the nonphasor behavior of the complex flux density explained earlier, the actual time variation of the flux density is also taken into account. At every time instant j, a real and positive error estimator is obtained from (11) as

$$h_{fj} = \left| \frac{1}{\mu_e} b_{tej} - \frac{1}{\mu_f} b_{tfj} \right|. \tag{12}$$

Corresponding error estimators h_{qj} and h_{rj} may again be defined for the other two neighbors q and r of element e and a maximum elementary estimator is computed as in (9).

The absolute value introduced in (12), like the square introduced in (8), simply prohibits negative error estimator values. The requirement of equidistribution of the error is also applied, the mean value h_{mj} of all h_j is calculated at every time instant j for all triangles of the current mesh, all triangles with $h_j \geq w h_{mj}$ are marked with a unitary integer flag and in the end, every element e will again be assigned a integer number equal to the sum of the corresponding n_T instantaneous integer flags. The advantages of this criterion, concerning flexibility and user intervention, are therefore the same described in the previous criterion.

C. Criterion #3: Instantaneous Energy of the Magnetic Field

The stored magnetic energy W in a linear and isotropic volume V is given by

$$W = \frac{1}{2\mu} \iiint_V \boldsymbol{B} \cdot \boldsymbol{B} \, dv. \tag{13}$$

Using the same 2-D FEM formulation of the quasi-static eddy-current problem defined in (1a)–(1c) and following the assumption of linear shape functions, the flux density is constant inside the element e having area S_e. Therefore, integrating (13) over the area S_e of element e, the elementary stored magnetic energy per unit length is derived as

$$W_e = \frac{1}{2\mu} \iint_{S_e} \boldsymbol{B} \cdot \boldsymbol{B} \, ds = \frac{|\boldsymbol{B}_e|^2 S_e}{2\mu}. \tag{14}$$

Since flux density is not a phasor, the mean value of stored magnetic energy in element e is not obtained easily from (14). Using the instantaneous values of the elementary flux density defined in (7c), the instantaneous value w_{ej} of the stored energy per unit length is derived from (14) as

$$w_{ej} = \frac{b_{ej}^2 S_e}{2\mu_0 \mu_{re}} \tag{15}$$

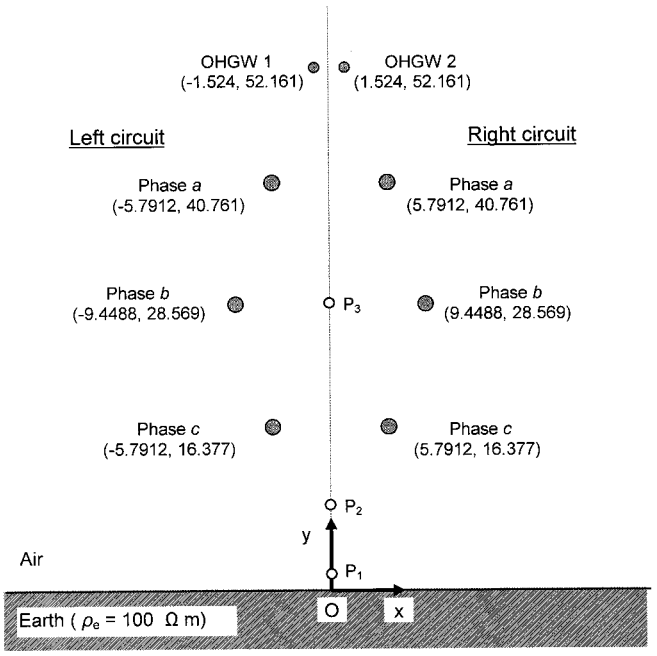

Fig. 2. Cross section of a double circuit transmission line (TL), having two overhead ground wires (OHGW). The center coordinates of each conductor and OHGW are given in meters.

and since the vacuum permeability is constant, an instantaneous real and positive local estimator h_j for the element e may be defined here as

$$h_j = \frac{b_{ej}^2 S_e}{\mu_{re}}. \tag{16}$$

The estimator defined in (16) is undoubtedly a clear and meaningful quantity. However, it must be pointed out that it does not represent an error estimator in a strict sense. Without having an analytical solution of the problem, there is no general way to precalculate h_j of (16) and therefore to make a comparison, in order to decide if element e has to be refined or not. However, FEM is a method mainly based on the minimization of energy. This minimization becomes better if the parts of the solution region having greater energy than others are thoroughly approximated. This leads to an adapted mesh having better equidistribution of the energy.

It must be also noticed that, between the different materials of the solution region, energy may take very different values [21]. Therefore, unlike the two previous criteria, the mean value h_{kmj} of all h_j given from (16) is now calculated at every j for all triangles of the current mesh that belong to the kth material. All triangles of the kth material having $h_j \geq w h_{kmj}$ are finally marked for refinement.

An additional computational advantage of this criterion, as compared to the first two criteria, is that a single real estimation is immediately computed for every element. Therefore, the calculation of the maximum estimator per element of (9) is omitted.

D. Criterion #4: Instantaneous Energy Density of the Magnetic Field

The last criterion is a slight variation of the previous one. The energy density of the magnetic field in a 2-D problem may be

TABLE I
TL SHOWN IN FIG. 2 WITH BALANCED LOAD: MAXIMUM VALUES OF THE RESULTANT FLUX DENSITY IN THREE POINTS P_1, P_2, AND P_3, LYING IN THE AXIS OF SYMMETRY OF THE TL. THE y COORDINATES OF THE POINTS ARE 1, 8, AND 28.569 m, RESPECTIVELY. THE FLUX DENSITIES HAVE BEEN CALCULATED BY FEM AFTER FOUR ITERATIONS, USING EACH OF THE FOUR CRITERIA. THE FEM VALUES ARE COMPARED TO THE CORRESPONDING REFERENCE MAXIMUM FLUX DENSITIES B_R, OBTAINED AT EVERY POINT FROM [26]

	B_R	B_{C1}	Error	B_{C2}	Error	B_{C3}	Error	B_{C4}	Error
	[mT]	[mT]	%	[mT]	%	[mT]	%	[mT]	%
P_1	16,60	17,02	2,53	21,92	32,05	16,73	0,78	21,83	31,51
P_2	26,57	27,97	5,27	21,92	-17,50	25,78	-2,97	21,83	-17,84
P_3	65,10	64,78	-0,49	65,48	0,58	64,70	-0,61	65,75	1,00

TABLE II
TL SHOWN IN FIG. 2 WITH BALANCED LOAD: DISTRIBUTION OF ELEMENTS IN THE DIFFERENT MATERIALS OF THE SOLUTION REGION, MEMORY ALLOCATED BY THE FEM SOLVER DURING THE FOURTH ITERATION AND TOTAL EXECUTION TIME REQUIRED BY THE FOUR ITERATIONS, FOR EACH OF THE FOUR DIFFERENT CRITERIA

Number of elements	Criterion #1	Criterion #2	Criterion #3	Criterion #4
Phase *a* conductor - left circuit	105	987	606	676
Phase *b* conductor - left circuit	108	960	606	661
Phase *c* conductor - left circuit	117	998	642	739
Phase *a* conductor - right circuit	108	988	632	673
Phase *b* conductor - right circuit	106	962	636	718
Phase *c* conductor - right circuit	114	992	660	717
OHGW 1	12	66	48	53
OHGW 2	12	63	60	72
Earth	344	60	646	320
Air	13271	10539	22385	9346
Total	14297	16615	26921	13975
Memory [Mbytes]	20	38	47	29
Execution time [min:sec]	04:25	07:27	08:22	04:53

considered as the energy per unit area, per unit length. If this area is the area of element e, this criterion results to an unweighted estimation of the magnetic energy, as compared to (14).

The magnetic energy density W_d in a 2-D problem defined in an area S is given by

$$W_d = \frac{1}{2\mu S} \iint_S \boldsymbol{B} \cdot \boldsymbol{B}\, ds. \tag{17}$$

Following again the assumption of linear shape functions and of constant flux density inside the element e and by integrating over the area S_e of element e, (17) leads to the elementary energy density W_{de}

$$W_{de} = \frac{|\boldsymbol{B}_e|^2}{2\mu}. \tag{18}$$

Using for the reasons explained earlier the instantaneous values of the elementary flux density defined in (7c), the instantaneous value w_{dej} of energy density derived from (18) is

$$w_{dej} = \frac{b_{ej}^2}{2\mu_0\mu_{re}} \tag{19}$$

and since the vacuum permeability is constant, an instantaneous real and positive local estimator h_j for the element e may be defined as

$$h_j = \frac{b_{ej}^2}{\mu_{re}}. \tag{20}$$

As in the previous criterion, the mean value h_{kmj} of all h_j given from (16) is calculated at every time instant j for all triangles of the current mesh that belong to the kth material. All triangles of the kth material having $h_j \geq wh_{kmj}$ are eligible for refining. The justifications as well as the advantages of this criterion are identical with those of the previous one.

IV. FINITE-ELEMENT MESH MANIPULATION

The local error estimators previously defined and their corresponding mean values are initially calculated, using an original coarse mesh and FEM solution. All elements with errors exceeding a predefined threshold percentage of each mean value are eligible for refinement. This refinement must not violate mesh consistency. After the refined mesh and the next FEM solution have been obtained, a number of checks has to be made in order to decide whether the mesh adaptation algorithms may

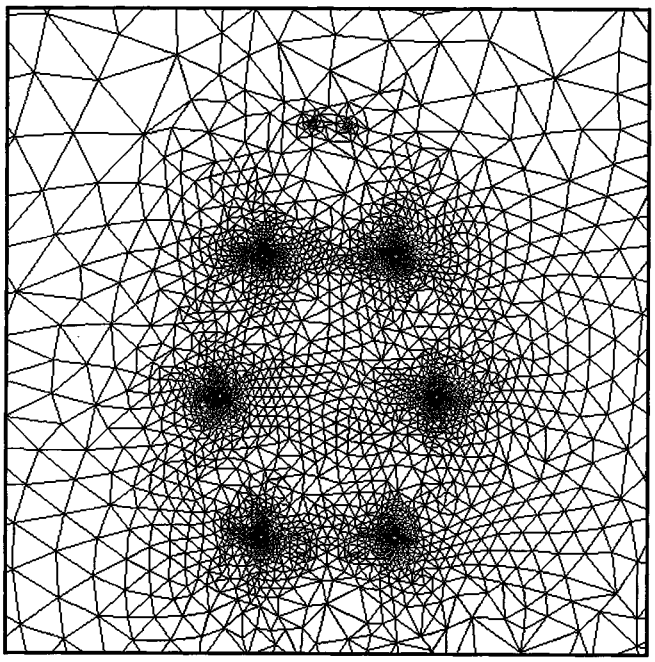

(a)

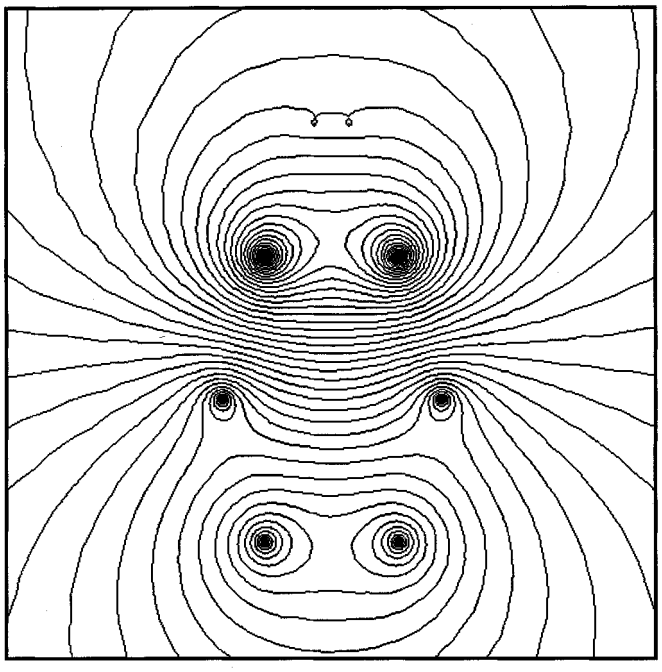

(b)

Fig. 3. (a) Finite-element mesh and (b) magnetic vector equipotentials at $\omega t = 0$ for the TL shown in Fig. 2 after the fourth iteration, using criterion #1.

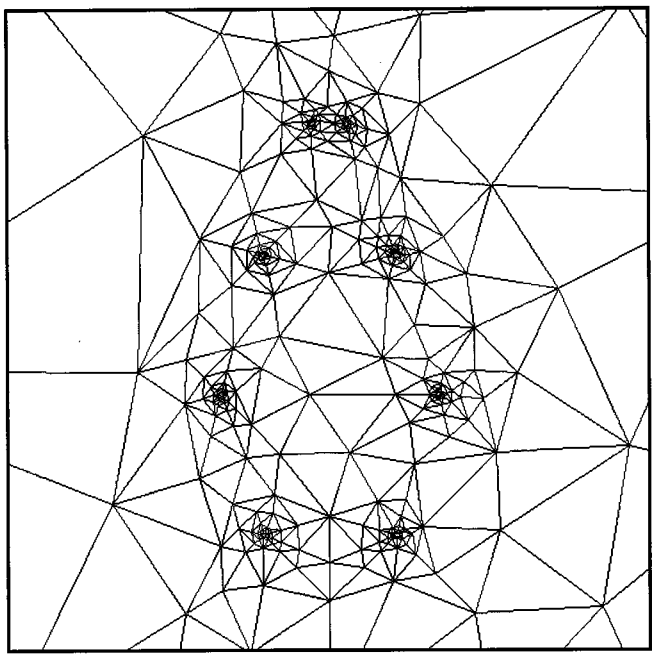

(a)

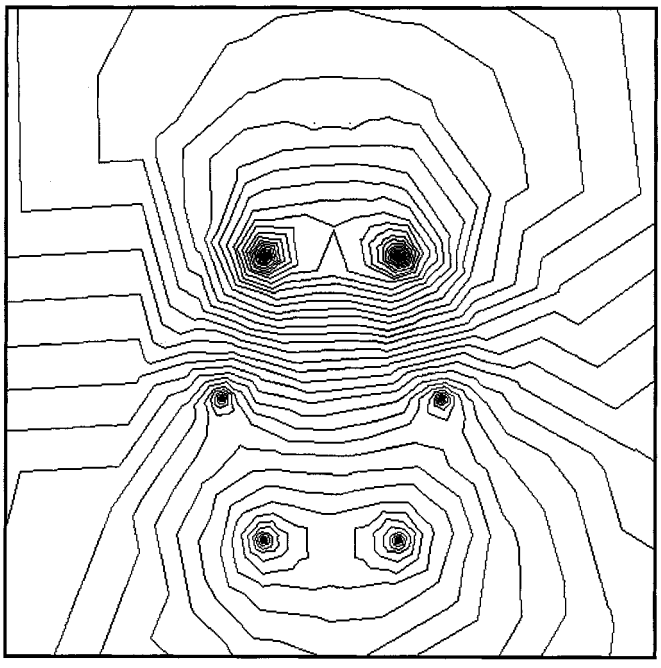

(b)

Fig. 4. (a) Finite-element mesh and (b) magnetic vector equipotentials at $\omega t = 0$ for the TL shown in Fig. 2 after the fourth iteration, using criterion #2.

proceed or not. These aspects along with some general directions are discussed in the following sections.

A. Element Subdivision

Once a triangle has been marked for refinement, three different element subdivision rules have been used, one for triangles having a side on an external boundary, a second for triangles lying on an internal boundary, and a third for all the other triangles.

- If a marked triangle has a side on an external (Dirichlet or Neumann) boundary, a new node is added at the midpoint of the boundary side. The original triangle is deleted and two new triangles are formed, using the new node and the three former triangle vertices.
- If a marked triangle has a side on an inside (interface) boundary between two different materials, a new node is added at the midpoint of the interface side. The two adjacent triangles are deleted and four new triangles are formed, using the new node and the four former triangle

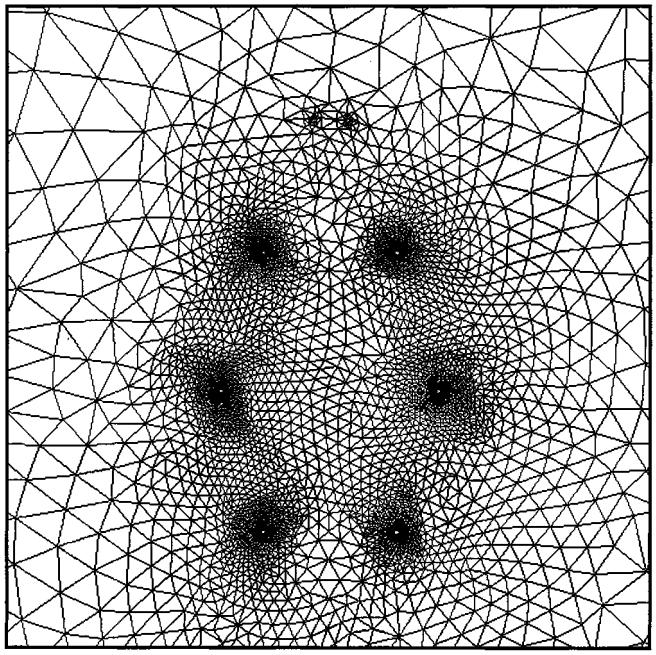

(a)

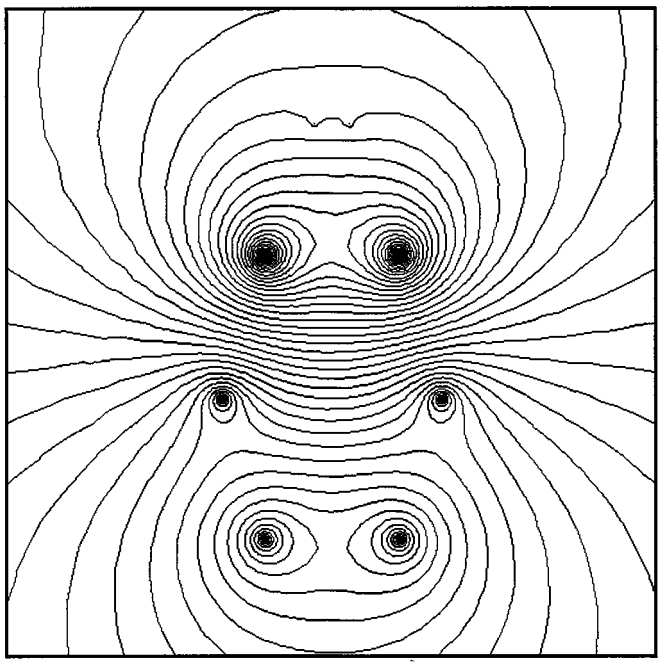

(b)

Fig. 5. (a) Finite-element mesh and (b) magnetic vector equipotentials at $\omega t = 0$ (b) for the TL shown in Fig. 2 after the fourth iteration, using criterion #3.

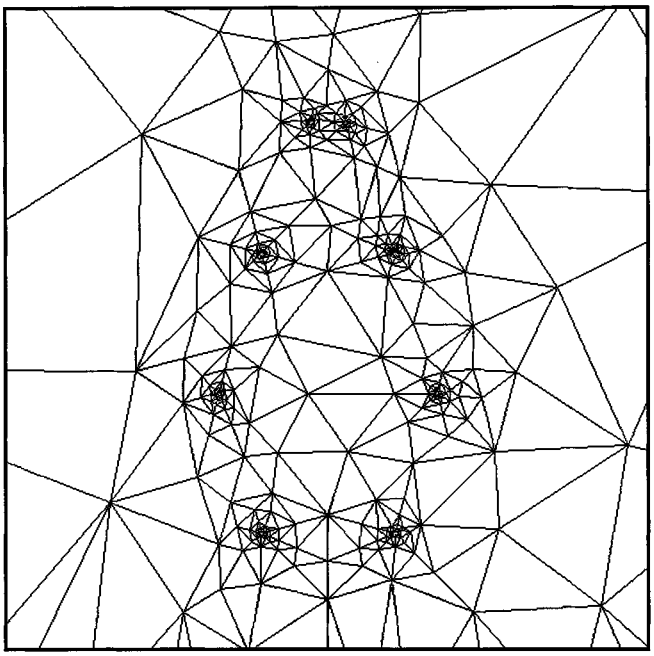

(a)

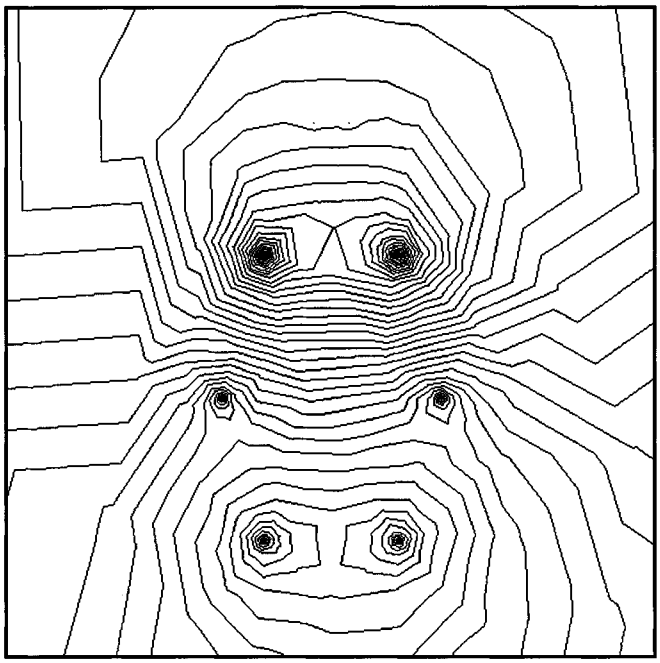

(b)

Fig. 6. (a) Finite-element mesh and (b) magnetic vector equipotentials at $\omega t = 0$ for the TL shown in Fig. 2 after the fourth iteration, using criterion #4.

vertices. Care has been taken in order to ensure that the new inserted node lies exactly on an explicitly defined curved interface and not simply at the midpoint of the interface side.

- If finally a marked triangle lies on the bulk, a new node is added in its centroid. The triangle is deleted and three new triangles are formed, using the new node and the three former triangle vertices.

Once the above rules have been applied to the whole mesh, a Delaunay triangulation is performed to provide an optimal mesh for the given set of nodes. The Delaunay triangulation follows the directions of [3], in order not to swap triangle edges across interface boundaries. Using the new optimally adapted mesh, a new FEM solution is calculated.

B. Termination Conditions

The procedure described previously is applied iteratively, until certain termination conditions are satisfied. These conditions are primarily imposed by the resources available on the computer used. A user may choose one of the following conditions.

TABLE III
TL SHOWN IN FIG. 2 WITH UNBALANCED LOAD: ZERO SEQUENCE IMPEDANCE PER UNIT LENGTH Z_{00} OF THE LEFT CIRCUIT OF THE TL, CALCULATED BY FEM AFTER FIVE ITERATIONS, USING EACH OF THE FOUR CRITERIA. THE FEM VALUES ARE COMPARED TO THE REFERENCE ZERO SEQUENCE IMPEDANCE PER UNIT LENGTH $Z_R = 0.286 + j1.067\ \Omega/\text{km}$, OBTAINED FROM [26]. NET CURRENTS AS WELL AS THE CORRESPONDING ERRORS COMPARED TO THE TOTAL 3000 A ZERO SEQUENCE GO CURRENT ARE ALSO SHOWN

	Criterion #1	Criterion #2	Criterion #3	Criterion #4
Z_{00} [Ω/km]	0.292 + j1.065	0.260 + j0.970	0.291 + j1.065	0.262 + j0.969
Re{Z_{00}} Error %	-2,10	9,09	-1,75	8,39
Im{Z_{00}} Error %	0,19	9,09	0,19	9,18
$\|I_{net}\|$ [A]	75,24	372,40	150,70	372,50
Error %	2,51	12,41	5,02	12,42

- The iterative procedure must stop if the memory resources of the computer are almost exhausted. This may be easily handled using a memory check in the end of each iteration, using the empirical rule that every subsequent mesh will need at least the double memory of the previous one.
- The iterative procedure must stop after a previously specified *number of iterations* n_i. This is usually the case when someone wants to compare different error estimators, in terms of the convergence of some operating parameter characterizing the solved problem.
- The iterative procedure must stop after a previously specified maximum execution time.
- The iterative procedure must stop if all triangles of the current mesh are marked for refinement. In this case, the desirable equidistribution of the error condition has been already met. A further subdivision of the mesh will probably add to the next FEM solution only a floating point computational error. Although this seems to be the best termination condition, it is unlikely to happen on a real geometrically complicated problem.

Indifferently of which of the first three above conditions has been met, the most recent solution must be available to the user in a form suitable to perform a next iteration, if it is still necessary.

V. EXAMPLES AND PERFORMANCE ANALYSIS

A. Common Values and Parameters

In all the examples presented in the following performance analysis, the rms current I_{rms}, the frequency f of the harmonic current, and the resistivity of the earth ρ_e are assumed to have the following values:

$$\begin{aligned} I_{\text{rms}} &= 1000\ \text{A} \\ f &= 50\ \text{Hz} \\ \rho_{\text{e}} &= 100\ \Omega\text{m} \end{aligned} \tag{21}$$

and remain constant, unless they are explicitly changed in a specific example. These constant values lead to a more precise evaluation of the performance of the four different criteria, since the corresponding estimators are sensitive to many of them.

Two other parameters that also remain constant in all criteria are the integer parameter w, defining the proportion of elements of the current mesh that will be marked for refinement and the integer number n_T used in time sampling computations. Concerning the first one, a value of $w = 1.1$ has been found to be a good compromise between speed and convergence. For the second one, a value of $n_T = 12$ has been proved to be a secure choice in all cases presented. Values less than six frequently lead to poor time sampling of the estimators, while values greater than 12 lead to unnecessary oversampling.

Having mainly in mind the accuracy of the solution in the presented examples, all the triangles set with an error flag greater than one have been selected for refinement. One of the advantages of the proposed method is that it allows the user to perform a quick problem solution using here values greater than one, or even the fastest through not so accurate solution, using a value equal to n_T.

All computations have been made using a Pentium computer at 233 MHz having 128 MB of memory. The operating system was Linux, the different criteria were C++ modules and they were easily incorporated in the FEM package developed by the author during the last 15 years.

B. Double Circuit Transmission Line—Balanced Case

The double circuit transmission line (TL), shown in Fig. 2, is initially considered. The two circuits are loaded with balanced harmonic currents, given in phasor notation by

$$\begin{aligned} I_{a\ \text{left}} &= \sqrt{2}I_{\text{rms}}e^{j0^\circ} & I_{a\ \text{right}} &= \sqrt{2}I_{\text{rms}}e^{j0^\circ} \\ I_{b\ \text{left}} &= \sqrt{2}I_{\text{rms}}e^{-j120^\circ} & I_{b\ \text{right}} &= \sqrt{2}I_{\text{rms}}e^{-j120^\circ} \\ I_{c\ \text{left}} &= \sqrt{2}I_{\text{rms}}e^{-j240^\circ} & I_{c\ \text{right}} &= \sqrt{2}I_{\text{rms}}e^{-j240^\circ}. \end{aligned} \tag{22}$$

The line is located over homogeneous earth with resistivity ρ_e. Eddy currents are induced in the earth as well as in the two grounded overhead ground wires (OHGW). The problem is solved using FEM with the four different criteria. An original coarse mesh consisting of 1915 elements has been used. Using the FEM solution, (2b) and (7c), the maximum values of the resultant flux density in three points (P_1, P_2, and P_3) have been calculated. The three points are located in the axis of symmetry of the line ($x = 0$), while their corresponding y coordinates are 1, 8, and 28.569 m, respectively.

TABLE IV
TL SHOWN IN FIG. 2 WITH UNBALANCED LOAD: DISTRIBUTION OF ELEMENTS IN THE DIFFERENT MATERIALS OF THE SOLUTION REGION, MEMORY ALLOCATED BY THE FEM SOLVER DURING THE FIFTH ITERATION AND TOTAL EXECUTION TIME REQUIRED BY THE FIVE ITERATIONS, FOR EACH OF THE FOUR DIFFERENT CRITERIA

Number of elements	Criterion #1	Criterion #2	Criterion #3	Criterion #4
Phase *a* conductor - left circuit	96	2790	1464	1890
Phase *b* conductor - left circuit	98	2814	1474	1898
Phase *c* conductor - left circuit	103	2763	1626	2038
Phase *a* conductor - right circuit	48	48	1564	2368
Phase *b* conductor - right circuit	48	48	1677	2329
Phase *c* conductor - right circuit	48	48	1724	2376
OHGW 1	63	864	81	90
OHGW 2	60	871	173	156
Earth	2536	60	2376	601
Air	16046	25087	34442	18489
Total	19146	35393	46601	32235
Memory [Mbytes]	28	102	107	129
Execution time [min:sec]	07:31	32:28	29:27	53:50

The FEM values are compared with those obtained from theoretical formulas, taken in this case from the most recent report of the IEEE Magnetic Fields Task Force of the Transmission and Distribution Committee [26]. The above comparison is shown in Table I, using as a termination condition the number of iterations $n_i = 4$. In this table, the flux density maximum values obtained from [26] have the subscript R, considered as reference, while the corresponding FEM obtained values have the composite subscript C along with the corresponding criterion number (i.e., from one to four). Criteria #1 and #3 present smaller errors than the other two, independently of the distance. Criteria #2 and #4 present small error only in the neighborhood of the phase conductors (point P_3), while this error increases rapidly when the point moves away from the high field region. Table II shows the distribution of elements in the different materials of the solution region, the memory allocated by the FEM solver during the fourth iteration as well as the execution time needed for the four iterations, for the four different criteria, respectively. It is remarkable that criterion #1 creates fewer elements per material, uses less memory, and therefore needs less execution time than criterion #3. The preferable criterion for this problem is therefore criterion #1. This conclusion may be emphasized by the corresponding meshes and magnetic vector equipotential plots shown in Figs. 3–6, which focus in the high field region near the current carrying conductors. The plots have been made with a constant MVP increment of 0.05×10^{-3} Wb/m. These figures also offer an explanation of the reasons the two other criteria (#2 and #4) produce significant errors, as shown in Table I. Although they generate a great number of triangles in the conductors, they build a very coarse mesh in the air surrounding them. On the other hand, criteria #1 and #3 present an adequate quality of magnetic vector equipotential lines.

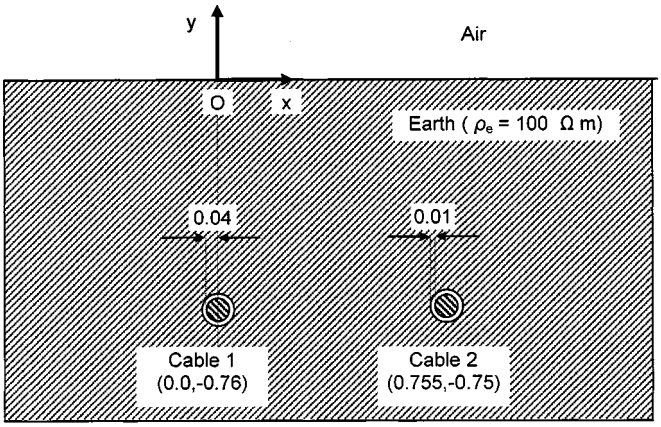

Fig. 7. Cross section of two underground insulated cables. The center coordinates of each of the two conductors are given in meters. Conductor radius is equal to 0.04 m and insulation thickness is 0.01 m.

C. Double Circuit Transmission Line—Unbalanced Case

The double circuit TL of Fig. 2 is now loaded with unbalanced currents. The left circuit is loaded with zero-sequence currents, while the right circuit is forced to carry zero currents. The currents are now given in phasor notation by

$$\begin{aligned} I_{a\,\text{left}} &= \sqrt{2} I_{\text{rms}} e^{j0^o} \quad I_{a\,\text{right}} = 0 \\ I_{b\,\text{left}} &= \sqrt{2} I_{\text{rms}} e^{j0^o} \quad I_{b\,\text{right}} = 0 \\ I_{c\,\text{left}} &= \sqrt{2} I_{\text{rms}} e^{j0^o} \quad I_{c\,\text{right}} = 0. \end{aligned} \tag{23}$$

The same original mesh, consisting of 1915 elements, has been initially used.

Using (23) and following the methodology presented in [27], FEM solution of (1a)–(1c) may lead directly to the computation of the symmetrical components impedance matrix for the TL. Values for the zero sequence impedance per unit length Z_{00} of

TABLE V

UNDERGROUND CABLE ARRANGEMENT SHOWN IN FIG. 7: MUTUAL IMPEDANCE PER UNIT LENGTH $Z_{12} = R_{12} + jX_{12}$, CALCULATED BY FEM FOR THREE DIFFERENT FREQUENCIES, USING EACH OF THE FOUR CRITERIA. TERMINATION CONDITION IS THE COMPUTER MEMORY, EQUAL TO 130 Mb. THE FEM VALUES ARE COMPARED TO THE REFERENCE MUTUAL IMPEDANCE PER UNIT LENGTH $Z_R = R_R + jX_R$, OBTAINED AT EVERY FREQUENCY FROM [29]. COMPARISON IS MADE FOR THE REAL AND FOR THE IMAGINARY PARTS OF Z_{12}, R_{12}, and X_{12}, RESPECTIVELY

	R_R	R_{C1}	Error	R_{C2}	Error	R_{C3}	Error	R_{C4}	Error
	[Ω/km]	[Ω/km]	%	[Ω/km]	%	[Ω/km]	%	[Ω/km]	%
f=100 Hz	0,09894	0,09883	-0,11	0,00151	-98,47	0,09629	-2,68	0,00148	-98,50
f=1000 Hz	0,9947	0,9938	-0,09	0,0024	-99,76	0,8622	-13,32	0,0015	-99,85
f=10000 Hz	10,101	10,089	-0,12	0,111	-98,90	4,476	-55,69	0,151	-98,50
	X_R	X_{C1}	Error	X_{C2}	Error	X_{C3}	Error	X_{C4}	Error
	[Ω/km]	[Ω/km]	%	[Ω/km]	%	[Ω/km]	%	[Ω/km]	%
f=100 Hz	0,85118	0,84977	-0,17	0,24504	-71,21	0,59532	-30,06	0,28111	-66,97
f=1000 Hz	7,0704	7,0439	-0,38	2,3560	-66,68	5,2740	-25,41	2,8210	-60,10
f=10000 Hz	56,403	55,858	-0,97	23,546	-58,25	37,046	-34,32	30,853	-45,30

TABLE VI

BUSBARS ARRANGEMENT SHOWN IN FIG. 8 WITH BALANCED LOAD: MAXIMUM VALUES OF ELECTROMAGNETIC FORCES PER UNIT LENGTH, ACTING ON THE CENTRAL CONDUCTOR (PHASE b). THE FORCES HAVE BEEN CALCULATED BY FEM AFTER NINE ITERATIONS, USING EACH OF THE FOUR CRITERIA. THE FEM VALUES ARE COMPARED TO THE CORRESPONDING REFERENCE MAXIMUM FORCES PER UNIT LENGTH $F_R = 2.0840$ N/m, OBTAINED FROM [31]

F_R	F_{C1}	Error	F_{C2}	Error	F_{C3}	Error	F_{C4}	Error
[N/m]	[N/m]	%	[N/m]	%	[N/m]	%	[N/m]	%
2,0840	2,0820	-0,10	1,8930	-9,17	2,0560	-1,34	1,2800	-38,58

TABLE VII

BUSBARS ARRANGEMENT SHOWN IN FIG. 8 WITH BALANCED LOAD: DISTRIBUTION OF ELEMENTS IN THE DIFFERENT MATERIALS OF THE SOLUTION REGION, MEMORY ALLOCATED BY THE FEM SOLVER DURING THE NINTH ITERATION AND TOTAL EXECUTION TIME REQUIRED BY THE NINE ITERATIONS, FOR EACH OF THE FOUR DIFFERENT CRITERIA

Number of elements	Criterion #1	Criterion #2	Criterion #3	Criterion #4
Phase *a* conductor	112	3664	1004	1591
Phase *b* conductor	234	3773	1131	1410
Phase *c* conductor	104	3746	693	565
Air	3858	7737	31798	22690
Total	4308	18920	34626	26256
Memory [Mbytes]	3	46	55	59
Execution time [min:sec]	02:09	12:49	17:11	14:41

the left circuit of the TL shown in Fig. 2 are presented here, using the four different criteria. The reference value for the zero sequence impedance per unit length is obtained from the line constants section of the well known electromagnetics transient program (EMTP) [28] and equals to $Z_{00} = 0.286 + j1.067\ \Omega/\text{km}$. The percent error for the real and imaginary parts of Z_{00} is shown in Table III, using again as a termination condition the number of iterations $n_i = 5$.

Because the load is now unbalanced, the net current I_{net}, which is the phasor sum of all currents in the different conducting materials, becomes an important operational parameter. Approximately 80% of the return current will flow in this case through earth, while the remaining portion will flow through the two OHGW's. Using an ideal mesh, I_{net} must approach to a zero magnitude phasor and therefore it may represent an additional estimation for the criterion used, concerning especially the mesh quality in the earth. Magnitude of the net cur-

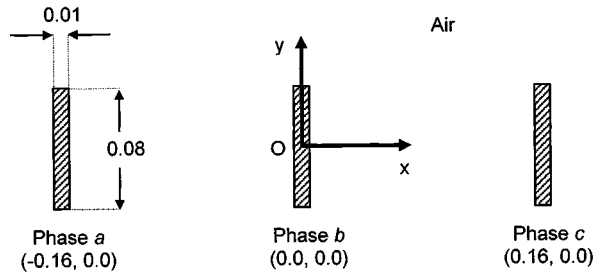

Fig. 8. Cross section of three rigid rectangular busbars. The center coordinates of each busbar are given in meters. Busbar height is equal to 0.08 m and its width is 0.01 m.

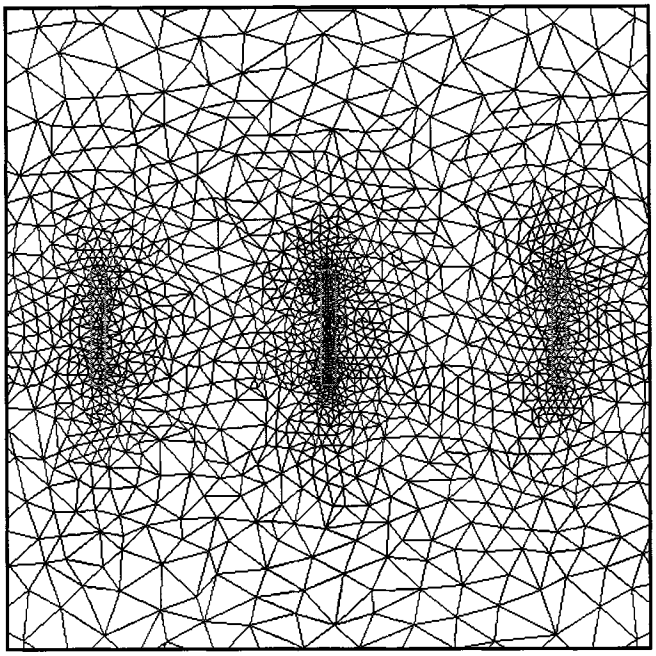

(a)

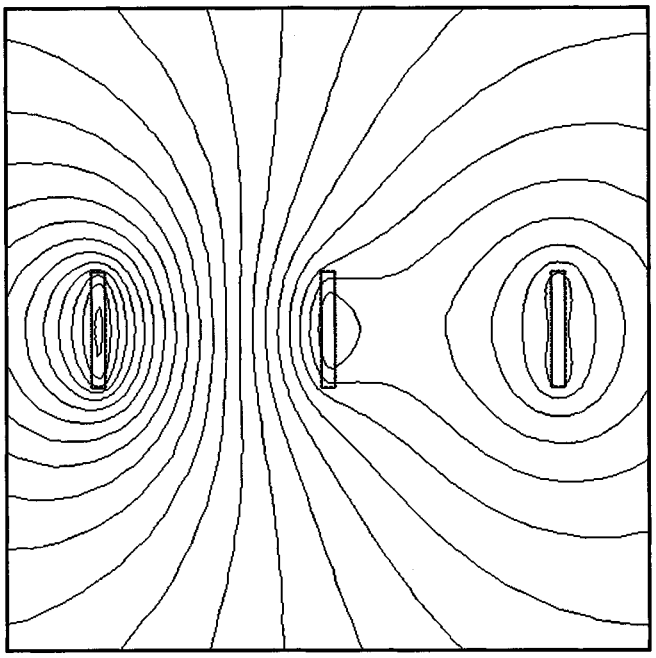

(b)

Fig. 9. (a) Finite-element mesh and (b) magnetic vector equipotentials at $\omega t = 0$ for the busbars shown in Fig. 8 after the ninth iteration, using criterion #1.

rent for every criterion as well as the corresponding errors are also shown in Table III. The % error reported is a fraction of the total conductors current, which in this case is the sum of the three zero-sequence currents $3I_{\rm rms} = 3000$ A.

Table IV shows the distribution of elements in the different materials of the solution region, the memory allocated by the FEM solver during the fifth iteration as well as the execution time needed for the five iterations, for each criterion. The small number of elements generated in earth by criteria #2 and #4 justify the net current errors of Table III. Also, criterion #3 generates unnecessarily a large number of elements inside the three conductors of the right circuit of the TL, leading to a larger memory requirement and to a larger total execution time comparing to criterion #1.

D. Mutual Impedance of Underground Cable System

The next problem examined, shown in Fig. 7, concerns the behavior of the different criteria in the calculation of the mutual impedance per unit length Z_{12} of two isolated underground cables. Three different frequencies have been chosen, 100, 1000, and 10 000 Hz, in order to test the estimators in varying skin depths. In order to compute Z_{12} by the method presented in [27], the two cables were loaded with unbalanced harmonics currents given in phasor notation by

$$I_1 = \sqrt{2} I_{\rm rms} e^{j0^\circ} \qquad I_2 = 0. \tag{24}$$

The integral relation given in [29] has been used to compute a reference value for the mutual impedance per unit length in this case. Numerical integration has been performed for the evaluation of the complex infinite integrals involved in [29]. For the FEM calculations, an original mesh consisting of 316 elements has been initially used. The reference values for the three frequencies, having the subscript R, as well as the values obtained using FEM with the different criteria, having the subscripts $C1$, $C2$, $C3$, and $C4$, are shown in Table V. Due to the difficulties introduced by the frequency variation, the termination condition used here was the exhaustion of the computer memory. Impedance values per unit length and corresponding errors are given separately for the real and the imaginary components of Z_{12}. Criterion #1 is evidently the only one that gives acceptable errors in this case. Criterion #3 leads to small errors in the $f = 100$ Hz case but fails for greater frequencies, the main reason for this being the poorly adapted mesh in the earth surrounding the two cables.

E. Electromagnetic Forces in Rigid Busbars

The last problem examined, shown in Fig. 8, concerns the calculation of electromagnetic forces acting on three-phase rigid busbars. The busbars are loaded with balanced harmonic currents, given in phasor notation by

$$\begin{aligned} I_a &= \sqrt{2} I_{\rm rms} e^{j0^\circ} \\ I_b &= \sqrt{2} I_{\rm rms} e^{-j120^\circ} \\ I_c &= \sqrt{2} I_{\rm rms} e^{-j240^\circ}. \end{aligned} \tag{25}$$

The forces per unit length calculated by FEM follow the approach presented in [30]. The maximum force per unit length F_{mb} acting on the central conductor (phase b) of Fig. 8 is only reported, since minor forces act on the outer conductors. The reference force per unit length in this case has been calculated using the relations given in the corresponding IEC Standard [31]. Using the geometry given in Fig. 8, (21) and (25) the reference maximum force per unit length is obtained from [31] as $F_{mb} = F_R = 2.0840$ N/m.

A coarse triangular mesh consisting of 62 elements has been initially used. Since in the methodology developed in [31] the earth influence is ignored, the corresponding problem solved by FEM and described by this mesh completely neglects earth

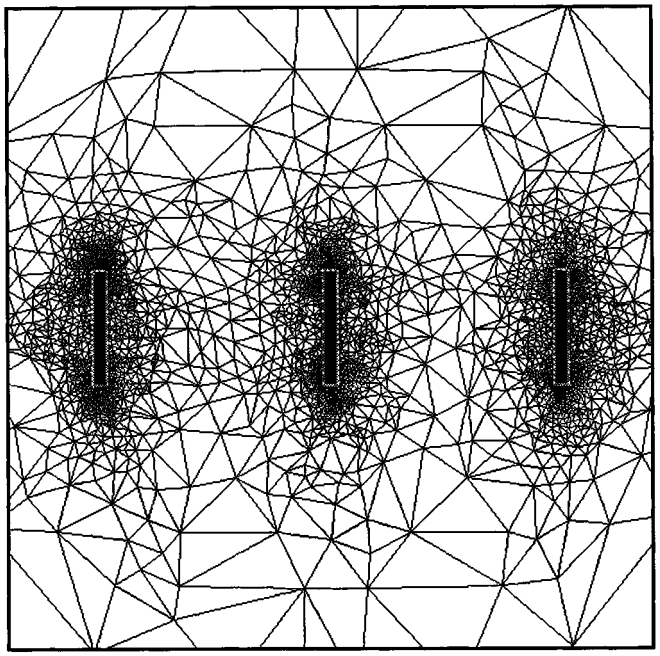

(a)

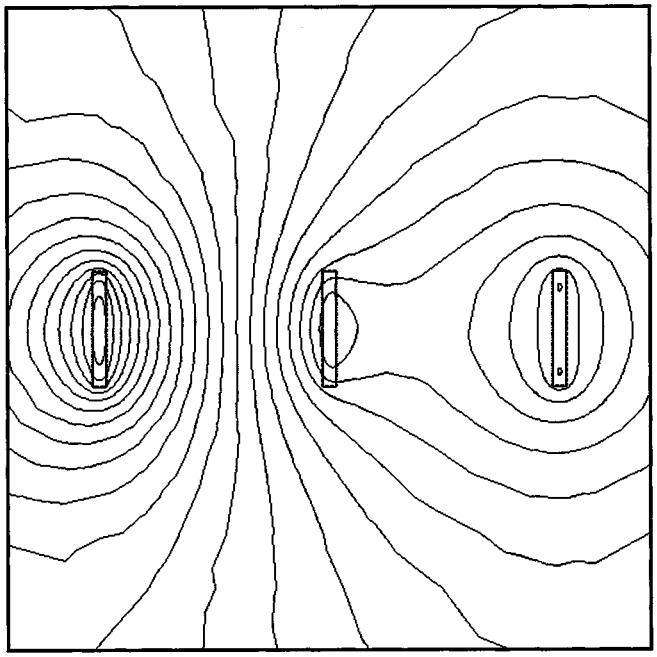

(b)

Fig. 10. (a) Finite-element mesh and (b) magnetic vector equipotentials at $\omega t = 0$ for the busbars shown in Fig. 8 after the ninth iteration, using criterion #2.

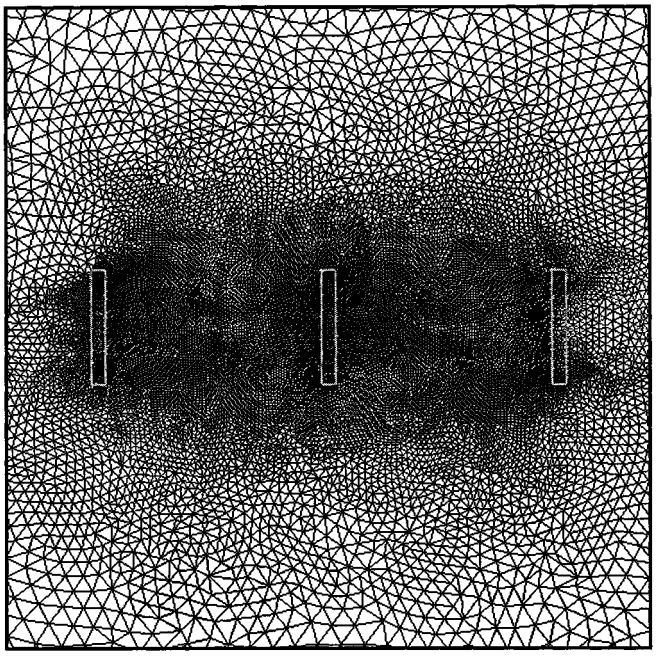

(a)

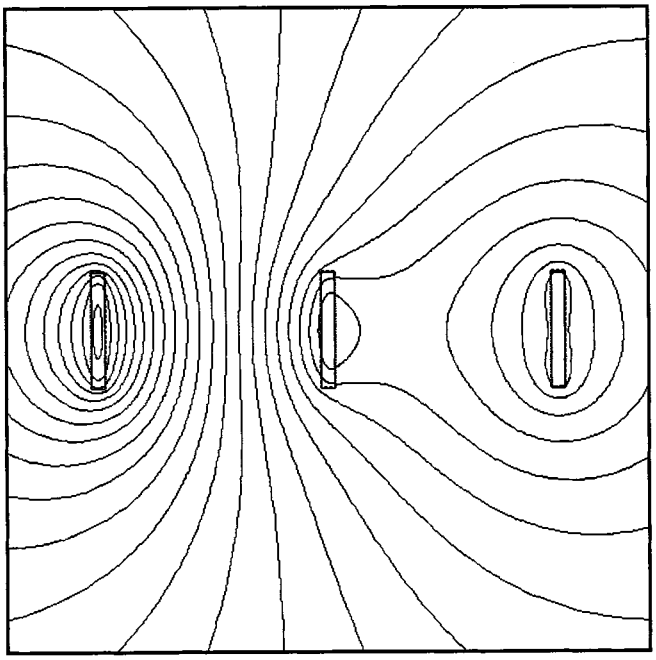

(b)

Fig. 11. (a) Finite-element mesh and (b) magnetic vector equipotentials at $\omega t = 0$ for the busbars shown in Fig. 8 after the ninth iteration, using criterion #3.

effects, in order to establish a consistent comparison. The reference maximum force per unit length F_R as well as the corresponding FEM values obtained by the different criteria are shown in Table VI. The termination condition used here was the number of iterations, specifically $n_i = 9$. Table VII shows the distribution of elements in the different materials of the solution region, the memory allocated by the FEM solver during the ninth iteration, as well as the execution time needed for the nine iterations, for each criterion. Criteria #1 and #3 produce acceptable percent errors, but as in all previous cases, criterion #1 generates the smallest mesh, needs only 3 Mb of memory for the ninth iteration, and therefore takes a much smaller execution time than criterion #3. This advantage of the criterion #1 allows the user to exhaust memory resources of the computer, if a better accuracy is required.

Finally, the corresponding meshes and magnetic vector equipotential plots are shown in Figs. 9–12, centered in the high field region near the busbars. The plots have been made

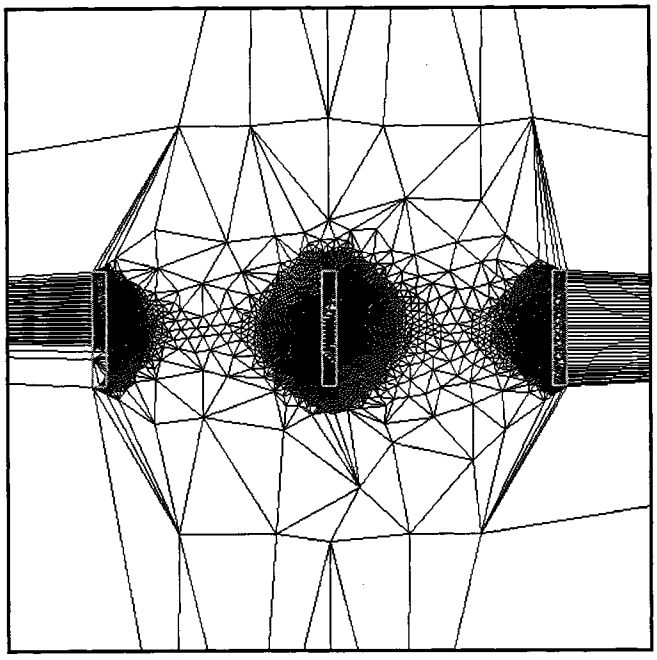

(a)

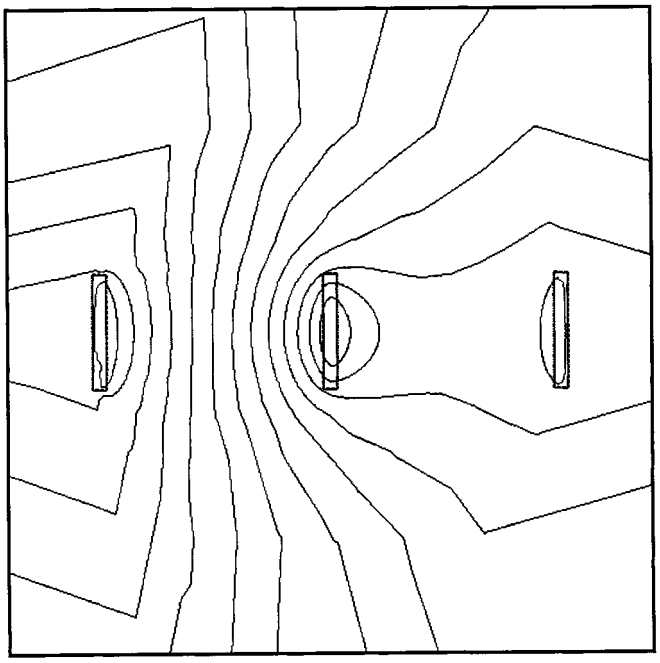

(b)

Fig. 12. (a) Finite-element mesh and (b) magnetic vector equipotentials at $\omega t = 0$ for the busbars shown in Fig. 8 after the ninth iteration, using criterion #4.

with a constant MVP increment of 0.05×10^{-3} Wb/m. Criteria #1 and #3 show again an adequate quality of magnetic vector equipotential lines. The same conclusions as in the balanced TL case, concerning the unnecessary creation of elements by criteria #2 and #4, also hold here.

VI. Conclusion

Four different criteria, introducing local error estimators for *a posteriori* h-type adaptive finite-element mesh generation are presented. The estimators are suitable for the solution of 2-D steady-state time harmonic quasi-static eddy-current problems, frequently encountered in electrical power transmission and distribution systems. The estimators are based on instantaneous field values, in order to overcome the difficulties introduced by the nonphasor behavior of field components.

The performance of the estimators has been investigated by solving various eddy-current problems. As a general conclusion, criterion #1, which is based on the discontinuity of the instantaneous tangential components of the magnetic field, has been proved satisfactory in all cases. It generates simple meshes, needs less computer resources, takes less time to converge, and always leads to acceptable errors. Criterion #3, based on the equidistribution of the instantaneous energy of the magnetic field, also leads to adequate results in many cases. However, it usually generates dense and memory consuming meshes, converges slowly, and fails when frequency is greater than 100 Hz. The other two criteria produce unacceptable meshes for all test cases and they must be avoided, at least for these kinds of problems.

Acknowledgment

The author wishes to thank Lecturer G. Papagiannis and D. Triantafyllidis of the Power Systems Laboratory at the Aristotle University of Thessaloniki, for their valuable help.

References

[1] O. C. Zienkiewicz and R. L. Taylor, *The Finite-Element Method*, ser. Basic Formulation and Linear Problems. London, U.K.: McGraw-Hill, 1989, vol. 1.

[2] E. E. Kriezis, T. D. Tsiboukis, S. M. Panas, and J. A. Tegopoulos, "Eddy currents: Theory and applications," *Proc. IEEE*, vol. 80, pp. 1559–1589, Oct. 1992.

[3] Z. J. Cendes, D. Shenton, and H. Shahnasser, "Magnetic field computation using Delaunay triangulation and complementary methods," *IEEE Trans. Magn.*, vol. MAG-19, pp. 2551–2554, Nov. 1983.

[4] J. Penman and M. D. Grieve, "An approach to self adaptive mesh generation," *IEEE Trans. Magn.*, vol. MAG-21, pp. 2567–2570, Nov. 1985.

[5] Z. J. Cendes and D. Shenton, "Adaptive mesh refinement in the finite-element computation of magnetic fields," *IEEE Trans. Magn.*, vol. MAG-21, pp. 1811–1816, Sept. 1985.

[6] A. R. Pinchuk and P. P. Silvester, "Error estimation for automatic adaptive finite-element mesh generation," *IEEE Trans. Magn.*, vol. MAG-21, pp. 2551–2554, Nov. 1985.

[7] J. Peraire, J. Peiro, L. Formaggia, K. Morgan, and O. C. Zienkiewicz, "Finite-element euler computations in three dimensions," *Int. J. Numer. Meth. Eng.*, vol. 26, pp. 2135–2159, 1988.

[8] P. Fernandes, P. Girdinio, P. Molfino, and M. Repetto, "Local error estimates for adaptive mesh refinement," *IEEE Trans. Magn.*, vol. MAG-24, pp. 299–302, Jan. 1988.

[9] S. Hahn, C. Calmels, G. Meunier, and J. L. Coulomb, "A posteriori error estimate for adaptive finite-element mesh refinement," *IEEE Trans. Magn.*, vol. MAG-24, pp. 315–317, Jan. 1988.

[10] A. Raizer, G. Meunier, and J. L. Coulomb, "An approach for automatic adaptive mesh refinement in finite-element computation of magnetic fields," *IEEE Trans. Magn.*, vol. 25, pp. 2965–2967, July 1989.

[11] N. A. Golias and T. D. Tsiboukis, "Adaptive refinement in 2-D finite-element applications," *Int. J. Nurner Mod. Electr. Dev. Fields*, vol. 4, pp. 81–95, 1991.

[12] P. Fernandes, P. Girdinio, P. Molfino, G. Molinari, and M. Repetto, "A comparison of adaptive strategies for mesh refinement based on *a posteriori* local error estimation procedures," *IEEE Trans. Magn.*, vol. 26, pp. 795–798, Mar. 1990.

[13] M. G. Vanti, A. Raizer, and J. P. A. Bastos, "A magnetostatic 2D comparison of local error estimators in FEM," *IEEE Trans. Magn.*, vol. 29, pp. 1902–1905, Mar. 1993.

[14] K. C. Chellamuthu and N. Ida, "Reliability assessment of an a posteriori error estimate for adaptive computation of electromagnetic field problems," *IEEE Trans. Magn.*, vol. 31, pp. 1761–1764, May 1995.
[15] J. Luomi and H. Rouhiainen, "Adaptive mesh refinement for magnetic field problems involving saturable ferromagnetic parts," *IEEE Trans. Magn.*, vol. MAG-24, pp. 311–314, Jan. 1988.
[16] S. McFee and J. P. Webb, "Adaptive finite-element analysis of microwave and optical devices using hierachal triangles," *IEEE Trans. Magn.*, vol. 28, pp. 1708–1711, Mar. 1992.
[17] M. Ziolkowski and H. Brauer, "Methods of mesh generation for biomagnetic problems," *IEEE Trans. Magn.*, vol. MAG-32, no. 3, pp. 1345–1348, May 1996.
[18] J. Ikdheimo, K. Forsman, and L. Kettunen, "Adaptive mesh generation in 3-D magnetostatic integral formulations," *IEEE Trans. Magn.*, vol. 33, pp. 1736–1739, Mar. 1997.
[19] N. A. Golias and T. D. Tsiboukis, "A-posteriori adaptive mesh refinement in the finite-element eddy-current computation," *COMPEL*, vol. 11, no. 1, pp. 249–252, 1992.
[20] K. C. Chellamuthu and N. Ida, "A posteriori element by element local error estimation technique and 2–D and 3–D adaptive finite-element mesh refinement," *IEEE Trans. Magn.*, vol. 30, pp. 3527–3530, Sept. 1994.
[21] P. Alotto, P. Girdinio, M. Nervi, and P. Fernandes, "Mesh adaptation in finite-element analysis of 2–D steady state time harmonic eddy-current problems," *IEEE Trans. Magn.*, vol. 32, no. 3, pp. 1361–1364, May 1996.
[22] P. Alotto, P. Girdinio, P. Molfino, and M. Nervi, "Time harmonic mesh adaption with error estimate based on the local field error approach," *IEEE Trans. Magn.*, vol. 33, pp. 1744–1747, Mar. 1997.
[23] A. Konrad, "Integrodifferential finite-element formulation of two-dimensional steady-state skin effect problems," *IEEE Trans. Magn.*, vol. MAG–18, pp. 284–292, Jan. 1982.
[24] J. Weiss and Z. Csendes, "A one-step finite-element method for multiconductor skin effect problems," *IEEE Trans. Power Appart. Syst.*, vol. PAS-101, pp. 3796–3803, Oct. 1982.
[25] G. Strang and G. J. Fix, *Analysis of The Finite-Element Method*. Cambridge, MA: Prentice-Hall, 1973.
[26] IEEE Committee Report, "Magnetic fields from electric power lines theory and comparison to measurements," *IEEE Trans. Power Delivery*, vol. PWRD-3, pp. 2127–2136, Oct. 1988.
[27] D. G. Triantafyllidis, G. K. Papagiannis, and D. P. Labridis, "Calculation of overhead transmission line impedances a finite-element approach," *IEEE Trans. Power Delivery*, vol. 14, pp. 287–293, Jan. 1999.
[28] *Electromagnetics Transients Program Reference Manual*, Bonneville Power Administration, Portland, OR, 1986, pp. 4.1–4.50.
[29] L. M. Wedepohl and D. J. Wilcox, "Transient analysis of underground power-transmission systems system-model and wave-propagation characteristics," *Proc. Inst. Elect. Eng.*, vol. 120, pp. 253–260, Feb. 1973.
[30] D. P. Labridis and P. S. Dokopoulos, "Electromagnetic forces in three-phase rigid busbars with rectangular cross-sections," *IEEE Trans. Power Delivery*, vol. 11, pp. 793–800, Apr. 1996.
[31] "Short-circuit currents—Calculation of effects. Part 1: Definitions and calculation methods," Bureau Central de la CEI, Geneve, Suisse, IEE-Publ. 865/1993.
[32] I. D. Mayergoyz, "A new approach to the calculation of three-dimensional skin effect problems," *IEEE Trans. Magn.*, vol. MAG-19, pp. 2198–2200, Sept. 1983.
[33] I. D. Mayergoyz, "3-D eddy-current problems and the boundary integral method," in *Computational Electromagnetics*. North-Holland, The Netherlands: Elsevier, 1986, pp. 163–171.

Dimitris P. Labridis (S'88–M'90) was born in Thessaloniki, Greece, on July 26, 1958. He received the Dipl.-Eng. degree and the Ph.D. degree from the Department of Electrical and Computer Engineering from the Aristotle University of Thessaloniki, in 1981 and 1989, respectively.

From 1982–1993 he worked, at first as a Research Assistant and later as a Lecturer, at the Department of Electrical and Computer Engineering at the Aristotle University of Thessaloniki, Greece. Since 1994, he has been an Assistant Professor in the same department. His special interests are power system analysis with special emphasis on the simulation of transmission and distribution systems, electromagnetic and thermal field analysis, numerical methods in engineering, and artificial intelligence applications in power systems.